Na-Ion Battery

International Edition: DOI: 10.1002/anie.201503188
German Edition: DOI: 10.1002/ange.201503188

Superior Na-Storage Performance of Low-Temperature-Synthesized $Na_3(VO_{1-x}PO_4)_2F_{1+2x}$ $(0 \le x \le 1)$ Nanoparticles for Na-Ion Batteries**

Yuruo Qi, Linqin Mu, Junmei Zhao, Yong-Sheng Hu,* Huizhou Liu,* and Sheng Dai*

Abstract: *Na-ion batteries are becoming comparable to Li-ion batteries because of their similar chemical characteristics and abundant sources of sodium. However, the materials production should be cost-effective in order to meet the demand for large-scale application. Here, a series of nanosized high-performance cathode materials, $Na_3(VO_{1-x}PO_4)_2F_{1+2x}$ $(0 \le x \le 1)$, has been synthesized by a solvothermal low-temperature (60–120 °C) strategy without the use of organic ligands or surfactants. The as-synthesized $Na_3(VOPO_4)_2F$ nanoparticles show the best Na-storage performance reported so far in terms of both high rate capability (up to 10 C rate) and long cycle stability over 1200 cycles. To the best of our knowledge, the current developed synthetic strategy for $Na_3(VO_{1-x}PO_4)_2F_{1+2x}$ is by far one of the least expensive and energy-consuming methods, much superior to the conventional high-temperature solid-state method.*

Renewable energy sources have numerous advantages compared with the three major traditional fossil fuels such as sustainability and that they are clean and pollution-free. Nevertheless, only 3% of today's energy is supplied from renewable and clean energy sources, such as solar power, wind, and waves, whereas nearly 68% is still obtained from the three major traditional fossil fuels.[1] To make the best use of these renewable energy sources, suitable energy-storage systems are the key. Among all alternative energy-storage technologies, efficient electrochemical systems are the most promising ones owing to their flexibility, high energy-conversion efficiency, and simple maintenance.

Due to their high energy and power density, Li-ion batteries (LIBs) nowadays occupy most of the portable electronic markets. Currently, the automotive industry is exploring LIBs as a power source for the next generation of EV and HEV. However, the high cost of lithium resulting from the low abundance and uneven distribution on Earth's crust remain a crucial limitation of LIBs for large-scale application. According to statistics, the price of lithium raw materials has roughly doubled from the end of the last century to the present, and it will continue to increase with the application of LIBs in automotive industry.[2] For comparison, sodium has chemical characteristics similar to those of lithium but sodium resources are abundant and widely distributed; therefore, Na-ion batteries (NIBs) are beginning to receive widespread attention, because it is believed that NIBs can compete with LIBs for large-scale energy-storage applications rather than portable electronic devices.

Up to now, layered transition metal oxides Na_xMO_2 (M = Fe, Co, Ni, Mn, Cu, etc.) and polyanionic compounds, such as $NaFePO_4$, $Na_3V_2(PO_4)_3$, Na_2FePO_4F, $NaV_{1-x}M_xPO_4F$ (M = Al, Cr), and $Na_3(VO_{1-x}PO_4)_2F_{1+2x}$ $(0 \le x \le 1)$ have been extensively explored as cathode materials for NIBs.[3] In particular, sodium vanadium fluorophosphates exhibit high storage capacity and high discharge voltage, making them attractive for high-energy NIBs.

Various methods for the preparation of sodium vanadium fluorophosphates and the investigation of their Na-storage properties as cathodes for NIBs have been reported. Among them, the solid-state high-temperature reaction became most popular since the $Na_3(VPO_4)_2F_3$ was firstly prepared by heating a mixture of NaF and VPO_4 at above 600 °C by Meins et al. in 1999.[4] Afterwards, the solid-state reaction was further coupled with other methods, such as a solid-state carbothermal reduction method (CTR)[3i,5] and a sol–gel process.[3t,u] However, the solid-state high-temperature reaction undoubtedly increases the cost of materials production. In addition, it has been reported that materials production is the main contribution to the total energy cost for producing an electrochemical storage system.[6]

To save energy and decrease the costs, there is a stringent need to expand the synthetic methods, shifting from high-temperature synthetic routes toward those that need comparably low temperature such as solvo-, hydro-, and ionothermal approaches. Most recently, Zhao et al. developed a phase-transfer-assisted low-temperature solvothermal strategy at a rather low temperature (80–140 °C) for the synthesis

[*] Y.-R. Qi,[+] Prof. J.-M. Zhao, Prof. H.-Z. Liu
Key Laboratory of Green Process and Engineering
Institute of Process Engineering, Chinese Academy of Sciences
Beijing 100190 (China)
E-mail: jmzhao@ipe.ac.cn
hzliu@ipe.ac.cn
Y.-R. Qi,[+]
University of Chinese Academy of Sciences
Beijing 100190 (China)
L.-Q. Mu[+] Prof. Y.-S. Hu
Beijing National Laboratory for Condensed Matter Physics
Institute of Physics, Chinese Academy of Sciences
Beijing 100190 (China)
E-mail: yshu@aphy.iphy.ac.cn
Prof. J.-M. Zhao, Prof. S. Dai
Chemical Sciences Division, Oak Ridge National Laboratory
Oak Ridge, TN 37831 (USA)
[+] These authors contributed equally to this work.

[**] The authors thank Yuesheng Wang for performing the XRD Rietveld refinement. This work was supported by Beijing Natural Science Foundation (2142030, 51222210) and the State Scholarship Fund from China Scholarship Council. S.D. was supported by the U.S. Department of Energy's Office of Basic Energy Science, Division of Materials Sciences and Engineering.
Supporting information for this article is available on the WWW under http://dx.doi.org/10.1002/anie.201503188.

of porous $Na_3(VO_{1-x}PO_4)_2F_{1+2x}$ (x = 0, 0.5, and 1) microspheres, and the as-synthesized products exhibit a good Na-storage performance.[7] Although it is a facile low-temperature one-step route and the as-synthesized materials show good electrochemical performance, an acid–base-coupled extractant (coupled by PC-88A and N1923, abbreviated as PN) was adopted in the synthetic process, in which the extractant PN loaded with H_3PO_4 was used as phosphate sources. Thus, the recycling extractant PN would inevitably increase the cost. Here, we further explore the possibility for optimizing the developed low-temperature solvothermal synthesis of $Na_3(VO_{1-x}PO_4)_2F_{1+2x}$ ($0 \le x \le 1$) without using the extractant PN.

Finally, using the proposed approach, we succeeded in the synthesis of $Na_3(VPO_4)_2F_3$ nanoparticles with particle sizes of 50–100 nm by one simple step at a rather low temperature (60–120 °C), just simply taking H_3PO_4 as phosphate source without any organic ligands or extractants. Due to the versatility of this approach, it can also be extended to synthesize a series of $Na_3(VO_{1-x}PO_4)_2F_{1+2x}$ ($0 \le x < 1$) compounds with similar particle sizes. The obtained materials show superior Na-storage performance in terms of both high rate capability and extremely stable cycling performance even without further carbon coating or high-temperature treatment. A simple graphical sketch on the current synthesis compared with the conventional method is shown in Figure 1,

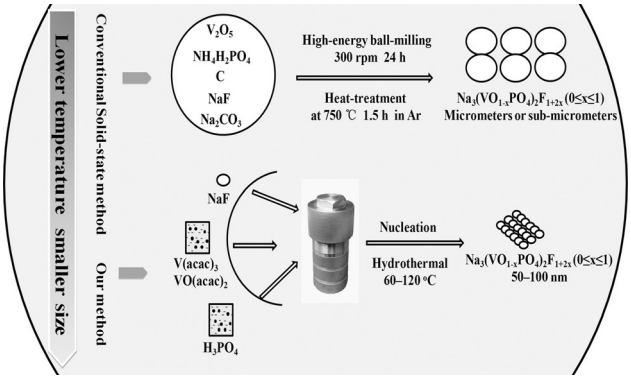

Figure 1. Graphical sketch of the current synthetic route compared with the conventional high-temperature solid-state method.

which embodies that the current developed synthetic strategy for $Na_3(VO_{1-x}PO_4)_2F_{1+2x}$ is much superior to the conventional high-temperature solid-state method.

The effects of several important parameters, such as the temperature of the solvothermal reaction, proportions of raw materials and reaction time, on the synthesis of the compound $Na_3(VPO_4)_2F_3$ were systematically investigated by evaluating the crystallinity, purity, and yields of products. Figure S1a shows the XRD patterns and yields of the as-synthesized $Na_3(VPO_4)_2F_3$ particles prepared starting from a molar ratio of 1:3:3 (V/P/F) at different temperatures (60 °C, 80 °C, 100 °C, 120 °C) for 10 h. As displayed in Figure S1a, the reaction temperature has no obvious impact on the purity and crystallinity but affects the yields of the products significantly. In fact, compound $Na_3(VPO_4)_2F_3$ can also be obtained at room temperature (RT) with a high yield of 96.5 %. However, reactions at RT require longer reaction times (around 20 days). It is interesting that the crystals can be formed at RT. This is the first report about the preparation of sodium vanadium fluorophosphates under such mild conditions. A detailed investigation on the preparation of these materials under even more mild conditions rather than the solvothermal route is currently underway. Here, in order to guarantee the high yields and accelerate the reaction rate, the solvothermal reaction at 120 °C was employed the optimization of other conditions, including proportions of raw materials and reaction time.

Figure S1b and S1c show the XRD patterns and yields of the as-synthesized $Na_3(VPO_4)_2F_3$ particles prepared at different molar ratios of V/P/F at 120 °C for 10 h. Similarly, different amounts of F or P have no obvious impact on the purity and crystallinity but only affect the yields of the products. From Figure S1b, various amounts of F demonstrate that a ratio of 1:1.67 for V/F is enough with a yield of 98.5 % whereas the ratio of V/P is fixed at 1:3. Conversely, as seen from Figure S1c, a ratio of 1:1.5 for V/P is enough with a yield of 98.8 % when the ratio of V/F is fixed at 1:1.67. On the basis of the yields and green synthesis viewpoint using as little raw materials as possible, the optimized ratio of V/P/F should be 1:1.5:1.67. Furthermore, the effect of reaction time on the preparation of $Na_3(VPO_4)_2F_3$ particles at 120 °C and 1:1.5:1.67 of V/P/F was investigated (Figure S1d). Different reaction times of 3 h, 5 h, 7 h, 10 h, 15 h, and 24 h were employed. Likewise, all of them can produce pure crystals but with different yields. Finally, the optimal time for the solvothermal reaction was found to be 10 h which gave a high yield of 98.8 %. The optimized reaction conditions for compound $Na_3(VPO_4)_2F_3$ are 120 °C, 1:1.5:1.67 of V/P/F, and a solvothermal reaction time of 10 h, and were used for the synthesis of $Na_3(VOPO_4)_2F$ and the series of $Na_3(VO_{1-x}PO_4)_2F_{1+2x}$ (x = 0.9, 0.7, 0.5, 0.3, 0.1) compounds.

Figure 2 presents the XRD patterns and FTIR spectra of the as-synthesized $Na_3(VO_{1-x}PO_4)_2F_{1+2x}$ (x = 1, 0.9, 0.7, 0.5, 0.3, 0.1, 0) samples recorded at room temperature. The corresponding enlarged views of these XRD patterns are also shown in Figure S2. Under the optimum conditions, all resulting samples $Na_3(VO_{1-x}PO_4)_2F_{1+2x}$ (x = 1, 0.9, 0.7, 0.5, 0.3, 0.1, 0) show a pure phase. No traces of impurities and intermediate phases are observed. It can be found that this series of $Na_3(VO_{1-x}PO_4)_2F_{1+2x}$ compounds can be obtained in the same crystal framework with a full range ($0 \le x \le 1$), which is confirmed by the similar XRD patterns. However, some subtle distinctions indeed do exist due to different compositions with varying amounts of F and O for $Na_3(VO_{1-x}PO_4)_2F_{1+2x}$ ($0 \le x \le 1$). For example, the major peaks can be indexed to (111), (002), (220), (113), (222), (400), (331), and (420) for $Na_3(VPO_4)_2F_3$ (x = 1) and (101), (002), (200), (103), (202), (220), (301), and (105) for $Na_3(VOPO_4)_2F$ (x = 0). According to the previous work, the two extreme members $Na_3(VPO_4)_2F_3$ (x = 1) and $Na_3(VOPO_4)_2F$ (x = 0) are composed of $V_2O_8F_3$ (V^{3+}) and $V_2O_{10}F$ (V^{4+}), respectively.[3i] In theory, the bond distance of V–O (1.63 Å) is shorter than that of V–F (2.0 Å), thus the lattice parameter c decreases with increasing ratio of O/F from $Na_3(VPO_4)_2F_3$

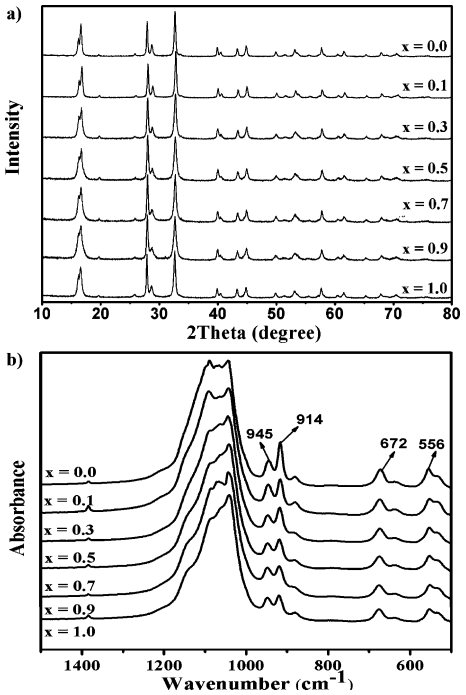

Figure 2. a) XRD patterns of the as-synthesized $Na_3(VO_{1-x}PO_4)_2F_{1+2x}$ ($x = 1.0, 0.9, 0.7, 0.5, 0.3, 0.1, 0$). b) FTIR spectra of the as-synthesized $Na_3(VO_{1-x}PO_4)_2F_{1+2x}$ ($x = 1.0, 0.9, 0.7, 0.5, 0.3, 0.1, 0$).

for $x = 1.0$ to $Na_3(VOPO_4)_2F$ for $x = 0$, which will lead to a continuous shift of part peaks toward a higher diffraction angle according to the Bragg equation. In fact, above analyses are confirmed by our experimental results. As examples, the peaks at 2θ of 16.6°, 27.9°, 28.7°, 51.3°, 55.4°, and 70.4°, which are indicated by asterisk (*) in Figure S2b and S2c, shift slightly to a higher 2θ at different degrees with an increasing ratio of O/F. These results are in good agreement with previous reports.[3i,7] The crystallite dimensions calculated from the Scherrer equation using Jade 6.0 software are ca. 30 nm (Table S1). As shown by TEM images (particle size is in the range of 50–100 nm), the as-synthesized nanoparticles belong to polycrystals and are composed of single-crystal granules, which is in agreement with the SAED results. In addition, the fitted profiles of $Na_3(VPO_4)_2F_3$ and $Na_3(VOPO_4)_2F$ were shown in Figure S3 and the corresponding fitted lattice parameters were also listed in Table S2.

The transition with an increasing ratio of O/F from $Na_3(VPO_4)_2F_3$ to $Na_3(VOPO_4)_2F$ can also be seen from the FTIR spectra. Figure 2b shows the FTIR spectra between 1500 cm^{-1} and 500 cm^{-1} for the as-synthesized $Na_3(VO_{1-x}PO_4)_2F_{1+2x}$ ($x = 1.0, 0.9, 0.7, 0.5, 0.3, 0.1, 0$) products. The strong broad band (1200–1000 cm^{-1}) can be attributed to asymmetric stretching of the PO_4^{3-} tetrahedron,[8] and the bands at 672 and 556 cm^{-1} can be assigned to P–O symmetric stretching and bending modes, respectively. It is clear that the relative strength of the bands at 945 and 914 cm^{-1} varies with increasing the ratio of O/F, which can be attributed to V–F[7] and V–O[9] stretching vibration modes, respectively. The vibration of V–F (945 cm^{-1}) becomes weaker when x decreases from 1 to 0, whereas the vibration of V–O (914 cm^{-1}) becomes stronger. There are two features that account for this continuous change. On one hand, the number of V–O increases with decreasing x, whereas the number of V–F gradually declines. According to Kang's work, the two extreme members $Na_3(VPO_4)_2F_3$ ($x = 1$) and $Na_3(VOPO_4)_2F$ ($x = 0$) are composed of $V_2O_8F_3$ and $V_2O_{10}F$, respectively. There are eight V–O bonds and four V–F bonds in $V_2O_8F_3$, and ten V–O bonds and two V–F bonds in $V_2O_{10}F$. The compounds $Na_3(VO_{1-x}PO_4)_2F_{1+2x}$ ($0 < x < 1$) could contain both $V_2O_8F_3$ (V^{3+}) and $V_2O_{10}F$ (V^{4+}), thereby the numbers of V–O bonds could gradually increase and V–F bonds decline slowly with decreasing x. On the other hand, the average bond distance of V–O decreases from 1.988 (in $V_2O_8F_3$ for $x = 1$) to 1.972 (in $V_2O_{10}F$ for $x = 0$), whereas that of V–F increases from 1.931 (in $V_2O_8F_3$ for $x = 1$) to 2.177 (in $V_2O_{10}F$ for $x = 0$).[3j] Therefore, the varied relative bond strength for V–F and V–O can be expected. Overall, some peak shift in XRD patterns and the varied relative strength for the bands at 945 and 914 cm^{-1} in the FTIR spectra confirm that V in compounds $Na_3(VO_{1-x}PO_4)_2F_{1+2x}$ ($0 \le x \le 1$) has a mixed valence of trivalence and tetravalence.

Furthermore, the particle sizes and typical morphologies of the as-synthesized family of $Na_3(VO_{1-x}PO_4)_2F_{1+2x}$ ($x = 1.0$, 0.9, 0.7, 0.5, 0.3, 0.1, 0) compounds were examined by SEM and TEM. As seen from Figure S4, the particle sizes are in the range of 50–100 nm. However, these nanosized particles are inclined to aggregate with the decrease of O/F, for example, the $Na_3(VOPO_4)_2F$ particles are more dispersive than $Na_3(VPO_4)_2F_3$. Interestingly, the $Na_3(VPO_4)_2F_3$ particles obtained at RT without the solvothermal method, display spherical particles with a size of hundreds of nanometers (Figure S4h), and are composed of smaller nanosized particles, which can be clearly seen from its TEM image (Figure S5f). However, the traditional high-temperature solid-state method usually generates microsized particles. Smaller size for material particles could be helpful in improving electrochemical properties because of the shorter diffusion distance and larger contact area with electrolyte. In addition, representative TEM images of $Na_3(VOPO_4)_2F$ and $Na_3(VPO_4)_2F_3$ synthesized by the solvothermal method were shown in Figure 3a and 3b, respectively. Other TEM images of $Na_3(VO_{1-x}PO_4)_2F_{1+2x}$ ($x = 0.9, 0.7, 0.5, 0.3, 0.1$) compounds were shown in Figure S5. All of these TEM images further confirm their nanosized feature. The typical high-resolution TEM (HRTEM) image and corresponding SAED pattern for $Na_3(VOPO_4)_2F$ in Figure 3c displays clear and continuous lattice planes, indicating the high crystallinity of the $Na_3(VOPO_4)_2F$ sample. The diffraction rings in the SAED pattern can be indexed to the (002), (103), (004), (213), (105), and (116) planes, attributed to the tetragonal phase of $Na_3(VOPO_4)_2F$. The distance (0.529 nm) between the adjacent lattice rings agrees well with the d spacing (002).[10] The results from SAED clearly indicate that the nano-polycrystals are assembled by single crystals with a tetragonal phase. Furthermore, elementary chemical composition of $Na_3(VOPO_4)_2F$, a model compound, was analyzed by energy-dispersive X-ray spectroscopy (EDS), as seen in Figure 3d. As the EDS spectrum shows, $Na_3(VOPO_4)_2F$ is composed of sodium, vanadium, phosphorus, fluorine, and oxygen without

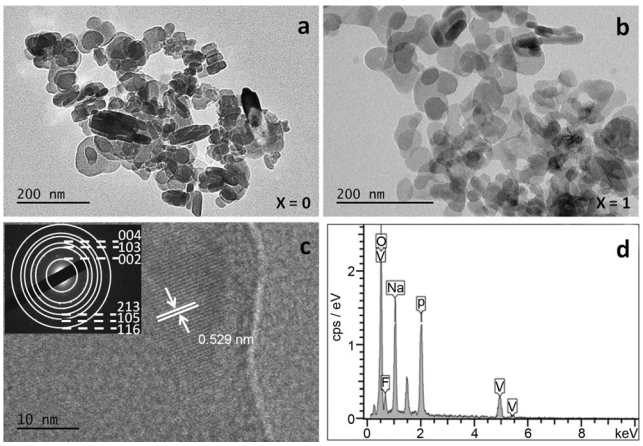

Figure 3. a) Typical TEM image for $Na_3(VOPO_4)_2F$ nanoparticles. b) Typical TEM image for $Na_3(VPO_4)_2F_3$ nanoparticles. c) Typical high-resolution TEM (HRTEM) image and corresponding SAED pattern for $Na_3(VOPO_4)_2F$ nanoparticles. d) The EDS pattern for $Na_3(VOPO_4)_2F$ nanoparticles.

other impurities and the molar ratio of these elements is in agreement with the molecular formula.

To understand the effect of fluorine content and oxidation state of vanadium on the electrochemical performance of these nanosized products, three representative products $Na_3(VPO_4)_2F_3$ ($x=1$), $Na_3(VO_{0.5}PO_4)_2F_2$ ($x=0.5$), and $Na_3(VOPO_4)_2F$ ($x=0$) were investigated with respect to Na-storage. The first discharge capacity of all three compounds $Na_3(VO_{1-x}PO_4)_2F_{1+2x}$ ($x=1.0$, 0.5, and 0) at a current rate of C/5 is over 110 mAh g^{-1}, as seen from the typical galvanostatic charge/discharge (Na extraction/insertion) curves (Figure 4a,b and S6). Moreover, a high first Coulombic efficiency of above 86% was achieved for all samples. In addition, all samples present two charge and discharge plateaus. The average discharge voltages are ca. 3.75 V for both samples. The energy density was calculated to be ca. 384 Wh kg^{-1}. The first difference between the two extreme members is that the charge and discharge plateaus for the $Na_3(VPO_4)_2F_3$ sample are located at 4.10 V/3.90 V and 3.70 V/3.50 V, whereas those for $Na_3(VOPO_4)_2F$ samples are 4.05 V/4.00 V and 3.65 V/3.60 V. The discharge voltage of the $Na_3(VOPO_4)_2F$ sample is slightly higher than that of $Na_3(VPO_4)_2F_3$ and the charge voltage of the $Na_3(VOPO_4)_2F$ sample is slightly lower than that of $Na_3(VPO_4)_2F_3$, thus the polarization of $Na_3(VOPO_4)_2F$ (0.05 V) is notably smaller than that of $Na_3(VPO_4)_2F_3$ (0.2 V). This result indicates better kinetics for Na extraction/insertion in $Na_3(VOPO_4)_2F$. The charge and discharge plateaus of $Na_3(VO_{0.5}PO_4)_2F_2$ ($x=0.5$; Figure S6) quite resemble those of $Na_3(VOPO_4)_2F$. It is worth noting that all these samples are prepared without further carbon coating and/or resorting to high-temperature treatment.

More importantly, all three nanosized samples revealed an outstanding cycling performance. After an initial discharge capacity of 110 mAh g^{-1} (for $Na_3(VPO_4)_2F_3$) and 112 mAh g^{-1} (for $Na_3(VOPO_4)_2F$), these nanosized products can achieve capacity retentions of 93.6% and 93.8% after 200 cycles at a current rate of C/5 (Figure 4a,b), respectively. To further confirm the excellent cycling performance, we performed long-term cycling experiments for both $Na_3(VPO_4)_2F_3$ ($x=1.0$) and $Na_3(VOPO_4)_2F$ ($x=0$) samples at a current rate of 2C displayed in Figure 4c,d. In both cases, the capacity retentions are still over 90% even after 1200 cycles which corresponds to a very small capacity decay of 0.008% per cycle, and Coulombic efficiency of above 99.5% can be obtained. In contrast to a previous work in which a poor cycle stability was reported for the tetravalence compound $Na_3(VOPO_4)_2F$,[3i] our nanosized sample shows extraordinary

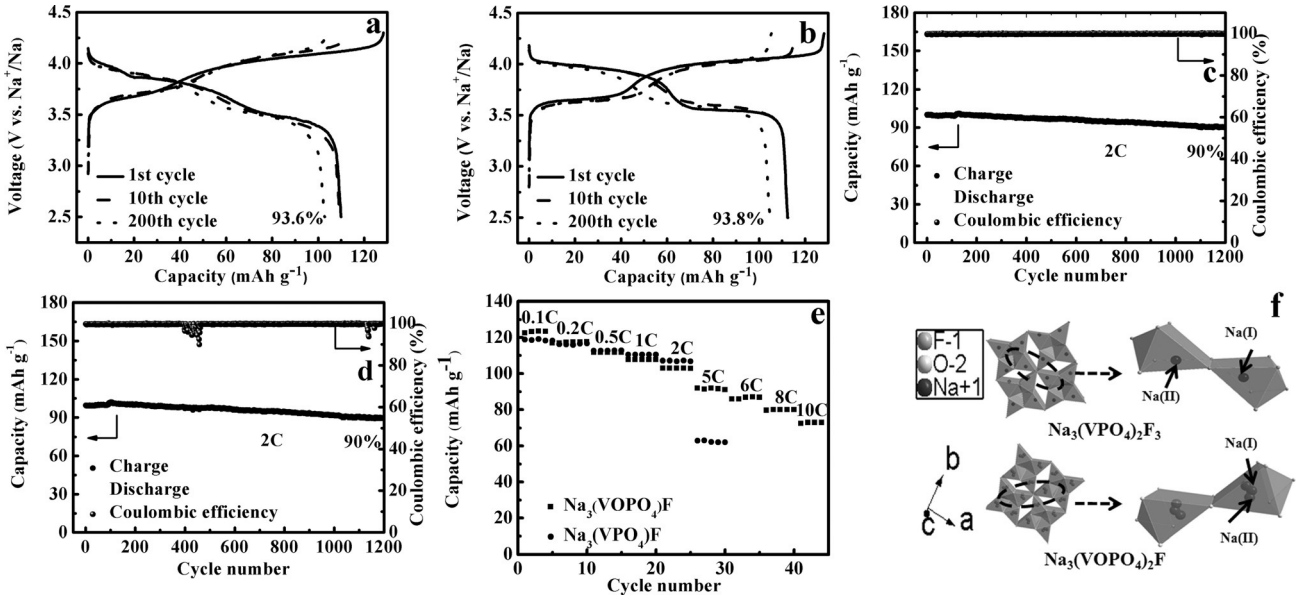

Figure 4. Galvanostatic charge and discharge curves of a) $Na_3(VPO_4)_2F_3$, b) $Na_3(VOPO_4)_2F$ electrodes cycled at a current rate of C/5 in the voltage range of 2.5–4.3 V. The cycling performance and Coulombic efficiency of c) $Na_3(VPO_4)_2F_3$ and d) $Na_3(VOPO_4)_2F$ electrodes at a current rate of 2C. (e) The rate capability of $Na_3(VPO_4)_2F_3$ and $Na_3(VOPO_4)_2F$ electrodes at various rates from C/10 to 10C. f) The coordination polyhedron around Na^+ ions in $Na_3(VPO_4)_2F_3$ and $Na_3(VOPO_4)_2F$.

cycling performance (Figure 4d). The long cycle stability is related to the very small volume change ($\approx 2\%$) during Na extraction and insertion.[3f,i,l,o] It has been demonstrated that small volume changes are favorable for improving the cycling performance.[11]

The rate capability of these two $Na_3(VPO_4)_2F_3$ ($x=1$) and $Na_3(VOPO_4)_2F$ ($x=0$) samples at current rates ranging from C/10 to 10C is displayed in Figure 4e. The discharge-specific capacities are 123.5, 117.7, 111.8, 107.7, 103, 91.8, 87, 79.9, 73 mAh g^{-1} for $Na_3(VOPO_4)_2F$ ($x=0$) at C/10, C/5, C/2, 1C, 2C, 5C, 6C, 8C, 10C, and 119.1, 116.7, 112.8, 110.5, 107.2, 63.1 mAh g^{-1} for $Na_3(VPO_4)_2F_3$ ($x=1$) at C/10, C/5, C/2, 1C, 2C, 5C, respectively. Both samples show a similar rate capability up to 2C, however, the discharge-specific capacity at 5C for $Na_3(VOPO_4)_2F$ ($x=0$) is maintained at 91.8 mAh g^{-1}(capacity retention is 74%), whereas that of $Na_3(VPO_4)_2F_3$ ($x=1$) is much lower (63.1 mAh g^{-1}, capacity retention is 53%). For the $Na_3(VOPO_4)_2F$ sample, under a very high rate of 10C (6 min charge/discharge), a reversible capacity of 73 mAh g^{-1} is achieved, corresponding to a capacity retention of 60%. High rate capability could be related to fast Na^+ ion diffusion and short transport distance. The transport distance of $Na_3(VOPO_4)_2F$ ($x=0$) is close to that of $Na_3(VPO_4)_2F_3$ ($x=1$) because of the comparative particle sizes. Therefore, the higher rate capability of $Na_3(VOPO_4)_2F$ ($x=0$) compared with that of $Na_3(VPO_4)_2F_3$ ($x=1$) could result from faster Na^+ ion diffusion in $Na_3(VOPO_4)_2F$. The coordination polyhedron around Na^+ ions (Figure 4f) show that seven negatively charged atoms (oxygen atoms and fluorine atoms) are around Na^+ for both compounds. However, there are three fluorine atoms and four oxygen atoms for $Na_3(VPO_4)_2F_3$ ($x=1$), and one fluorine atom and six oxygen atoms for $Na_3(VOPO_4)_2F$ ($x=0$). It is well known that the electronegativity of fluorine and oxygen atoms is different and that stronger electronegativity of fluorine atoms would produce stronger attraction interaction for Na^+ ions as confirmed by the shorter bond of Na2–F2 in $Na_3(VPO_4)_2F_3$ ($x=1$) compared with that of Na2–O2 in $Na_3(VOPO_4)_2F$ ($x=0$; Figure S7), which may restrict the diffusion of Na^+ ions.[3h–j,o–q,12] The number of fluorine atoms for $Na_3(VOPO_4)_2F$ ($x=0$) is less than that of $Na_3(VPO_4)_2F_3$ ($x=1$), thereby faster Na^+ ion diffusion could be expected for $Na_3(VOPO_4)_2F$ ($x=0$) even though its crystal structure is similar to that of $Na_3(VPO_4)_2F_3$ ($x=1$). To the best of our knowledge, the resulting $Na_3(VOPO_4)_2F$ ($x=0$) nanoparticles exhibit the best Na-storage performance so far in terms of both long cycle stability and high rate capability.[3i,j,l–n,p–r,13]

In conclusion, we have developed a facile one-step solvothermal route for the synthesis of a family of nanosized compounds $Na_3(VO_{1-x}PO_4)_2F_{1+2x}$ ($0 \le x \le 1$) at a rather low temperature between 60 and 120°C that does not require organic ligands or surfactants. Interestingly, even at room temperature, the reaction can occur spontaneously with a rather high yield of 96.5% within dozens of days. Taking $Na_3(VPO_4)_2F_3$ as a model compound, the reaction conditions were optimized by evaluating the crystallinity, purity, and yields of products. The optimized reaction conditions (120°C, 1:1.5:1.67 of V/P/F, and solvothermal reaction time of 10 h) can be further extended to prepare other representative compounds $Na_3(VO_{1-x}PO_4)_2F_{1+2x}$ ($x=0.9, 0.7, 0.5, 0.3, 0.1, 0$). The particle sizes of the resulting products are in the range of 50–100 nm. The representative compounds $Na_3(VOPO_4)_2F$ exhibit a specific capacity of 112 mAh g^{-1} at a current rate of C/5 with an average operation voltage of 3.75 V. The most prominent properties are the extraordinary cycling performance with 90% capacity retention over 1200 cycles at a 2C rate and the outstanding rate capability with a specific capacity of 73 mAh g^{-1} (60% capacity retention) at a 10C rate (6 min charge/discharge). A higher rate capability is achieved for the $Na_3(VOPO_4)_2F$ sample compared with that of $Na_3(VPO_4)_2F_3$, which could be related to a possibly faster Na^+-ion diffusion for $Na_3(VOPO_4)_2F$. Compared with the conventional two-step high-temperature processes, this low-temperature solvothermal approach would undoubtedly decrease the cost of material fabrication significantly and could be expanded as a general strategy for the synthesis of other electrode materials.

Keywords: cathode · $Na_3(VOPO_4)_2F$ · Na-ion batteries · nanoparticles · solvothermal synthesis

How to cite: *Angew. Chem. Int. Ed.* **2015**, *54*, 9911–9916
Angew. Chem. **2015**, *127*, 10049–10054

[1] Z. Yang, J. Zhang, M. C. Kintner-Meyer, X. Lu, D. Choi, J. P. Lemmon, J. Liu, *Chem. Rev.* **2011**, *111*, 3577–3613.

[2] a) N. Yabuuchi, K. Kubota, M. Dahbi, S. Komaba, *Chem. Rev.* **2014**, *114*, 11636–11682; b) M. D. Slater, D. Kim, E. Lee, C. S. Johnson, *Adv. Funct. Mater.* **2013**, *23*, 947–958; c) H. Pan, Y.-S. Hu, L. Chen, *Energy Environ. Sci.* **2013**, *6*, 2338–2360; d) V. Palomares, M. Casas-Cabanas, E. Castillo-Martínez, M. H. Han, T. Rojo, *Energy Environ. Sci.* **2013**, *6*, 2312–2337; e) S.-W. Kim, D.-H. Seo, X. Ma, G. Ceder, K. Kang, *Adv. Energy Mater.* **2012**, *2*, 710–721.

[3] a) H. Yu, S. Guo, Y. Zhu, M. Ishida, H. Zhou, *Chem. Commun.* **2014**, *50*, 457–459; b) K. Kubota, N. Yabuuchi, H. Yoshida, M. Dahbi, S. Komaba, *MRS Bull.* **2014**, *39*, 416–422; c) S. Guo, H. Yu, P. Liu, Y. Ren, T. Zhang, M. Chen, M. Ishida, H. Zhou, *Energy Environ. Sci.* **2015**, *8*, 1237–1244; d) L. Q. Mu, Y. S. Hu, L. Q. Chen, *Chin. Phys. B* **2015**, *24*, 038202; e) J. Barker, M. Saidi, J. Swoyer, *Electrochem. Solid-State Lett.* **2003**, *6*, A1–A4; f) K. Chihara, A. Kitajou, I. D. Gocheva, S. Okada, J.-i. Yamaki, *J. Power Sources* **2013**, *227*, 80–85; g) R. Gover, A. Bryan, P. Burns, J. Barker, *Solid State Ionics* **2006**, *177*, 1495–1500; h) Z. Liu, Y.-Y. Hu, M. T. Dunstan, H. Huo, X. Hao, H. Zou, G. Zhong, Y. Yang, C. P. Grey, *Chem. Mater.* **2014**, *26*, 2513–2521; i) Y. U. Park, D. H. Seo, H. Kim, J. Kim, S. Lee, B. Kim, K. Kang, *Adv. Funct. Mater.* **2014**, *24*, 4603–4614; j) Y. U. Park, D. H. Seo, H. S. Kwon, B. Kim, J. Kim, H. Kim, I. Kim, H. I. Yoo, K. Kang, *J. Am. Chem. Soc.* **2013**, *135*, 13870–13878; k) A. Ponrouch, R. Dedryvère, D. Monti, A. E. Demet, J. M. Ateba Mba, L. Croguennec, C. Masquelier, P. Johansson, M. R. Palacín, *Energy Environ. Sci.* **2013**, *6*, 2361–2369; l) P. Serras, V. Palomares, J. Alonso, N. Sharma, J. M. López del Amo, P. Kubiak, M. L. Fdez-Gubieda, T. Rojo, *Chem. Mater.* **2013**, *25*, 4917–4925; m) P. Serras, V. Palomares, A. Goñi, I. Gil de Muro, P. Kubiak, L. Lezama, T. Rojo, *J. Mater. Chem.* **2012**, *22*, 22301–22308; n) P. Serras, V. Palomares, A. Goñi, P. Kubiak, T. Rojo, *J. Power Sources* **2013**, *241*, 56–60; o) R. Shakoor, D.-H. Seo, H. Kim, Y.-U. Park, J. Kim, S.-W. Kim, H. Gwon, S. Lee, K. Kang, *J. Mater. Chem.* **2012**, *22*, 20535–20541; p) W. Song, X. Cao, Z. Wu, J. Chen, Y. Zhu, H. Hou, Q. Lan, X. Ji, *Langmuir* **2014**, *30*, 12438–12446; q) W. Song, X. Ji, Z. Wu, Y. Yang, Z. Zhou, F. Li,

Q. Chen, C. E. Banks, *J. Power Sources* **2014**, *256*, 258 – 263; r) W. Song, X. Ji, Z. Wu, Y. Zhu, F. Li, Y. Yao, C. E. Banks, *RSC Adv.* **2014**, *4*, 11375 – 11383; s) H. Zhuo, X. Wang, A. Tang, Z. Liu, S. Gamboa, P. Sebastian, *J. Power Sources* **2006**, *160*, 698 – 703; t) J. Zhao, J. He, X. Ding, J. Zhou, Y. o. Ma, S. Wu, R. Huang, *J. Power Sources* **2010**, *195*, 6854 – 6859; u) T. Jiang, G. Chen, A. Li, C. Wang, Y. Wei, *J. Alloys Compd.* **2009**, *478*, 604 – 607; v) Y. Cao, L. Xiao, W. Wang, D. Choi, Z. Nie, J. Yu, L. V. Saraf, Z. Yang, J. Liu, *Adv. Mater.* **2011**, *23*, 3155 – 3160.

[4] J.-M. Le Meins, M.-P. Crosnier-Lopez, A. Hemon-Ribaud, G. Courbion, *J. Solid State Chem.* **1999**, *148*, 260 – 277.

[5] J. Barker, R. Gover, P. Burns, A. Bryan, *Electrochem. Solid-State Lett.* **2006**, *9*, A190 – A192.

[6] D. Larcher, J. Tarascon, *Nat. Chem.* **2015**, *7*, 19 – 29.

[7] J. Zhao, L. Mu, Y. Qi, Y.-S. Hu, H. Liu, S. Dai, *Chem. Commun.* **2015**, *51*, 7160 – 7163.

[8] F. Sauvage, E. Quarez, J.-M. Tarascon, E. Baudrin, *Solid State Sci.* **2006**, *8*, 1215 – 1221.

[9] L. D. Frederickson, Jr., D. Hausen, *Anal. Chem.* **1963**, *35*, 818 – 827.

[10] W. M. O. V. Y. O. V. Dimitrova, *Solid State Sci.* **2002**, *4*, 495 – 501.

[11] Y. Wang, X. Yu, S. Xu, J. Bai, R. Xiao, Y. S. Hu, H. Li, X. Q. Yang, L. Chen, X. Huang, *Nat. Commun.* **2013**, *4*, 2365.

[12] M. Xu, P. Xiao, S. Stauffer, J. Song, G. Henkelman, J. B. Goodenough, *Chem. Mater.* **2014**, *26*, 3089 – 3097.

[13] M. Peng, B. Li, H. Yan, D. Zhang, X. Wang, D. Xia, G. Guo, *Angew. Chem. Int. Ed.* **2015**, *54*, 6452 – 6456; *Angew. Chem.* **2015**, *127*, 6552 – 6556.

Received: April 7, 2015
Published online: July 14, 2015

